Research Article | Vol. 8, No. 2 | 1 Feb 2017 | BIOMEDICAL OPTICS EXPRESS 1110
Biomedical Optics EXPRESS

VCSEL-based swept source for low-cost optical coherence tomography

SUCBEI MOON[1,*] AND EUN SEO CHOI[2]

[1]*Department of Physics, Kookmin University, Seoul, 02707, South Korea*
[2]*Department of Physics, Chosun University, Gwangju, 61452, South Korea*
**moons@kookmin.ac.kr*

Abstract: We present a novel wavelength-swept laser source for optical coherence tomography (OCT) which is based on the conventional laser diode technology of the vertical-cavity surface-emitting laser (VCSEL). In our self-heating sweep VCSEL (SS-VCSEL), a VCSEL device is simply driven by ramped pulses of currents in direct intensity modulation. The intrinsic property of VCSEL produces a frequency-swept output through the self-heating effect. By the injected current, the temperature of the active region is gradually increased in this effect. Consequently, it changes the wavelength of the laser output by itself. In this study, various characteristics of our SS-VCSEL were experimentally investigated for low-cost instrumentation of a swept source OCT system. A low-cost SS-VCSEL-based OCT system was demonstrated in this research that provided an axial resolution of 135 μm in air, sensitivity of −91 dB and a maximum imaging range longer than 10 cm when our source was operated at a sweep repetition rate of 5 kHz with an output power of 0.41 mW. Based on the experimental observations, we believe that our SS-VCSEL swept source can be an economic alternative in some of low-cost or long-range applications of OCT.

OCIS codes: (110.4500) Optical coherence tomography; (140.7260) Vertical cavity surface emitting lasers; (170.4500) Optical coherence tomography.

References and links

1. S. Yun, G. Tearney, J. de Boer, N. Iftimia, and B. Bouma, "High-speed optical frequency-domain imaging," Opt. Express **11**(22), 2953–2963 (2003).
2. S. R. Chinn, E. A. Swanson, and J. G. Fujimoto, "Optical coherence tomography using a frequency-tunable optical source," Opt. Lett. **22**(5), 340–342 (1997).
3. R. Huber, M. Wojtkowski, and J. G. Fujimoto, "Fourier Domain Mode Locking (FDML): A new laser operating regime and applications for optical coherence tomography," Opt. Express **14**(8), 3225–3237 (2006).
4. R. Huber, D. C. Adler, and J. G. Fujimoto, "Buffered Fourier domain mode locking: Unidirectional swept laser sources for optical coherence tomography imaging at 370,000 lines/s," Opt. Lett. **31**(20), 2975–2977 (2006).
5. S. Moon and D. Y. Kim, "Ultra-high-speed optical coherence tomography with a stretched pulse supercontinuum source," Opt. Express **14**(24), 11575–11584 (2006).
6. J. Xu, X. Wei, L. Yu, C. Zhang, J. Xu, K. K. Wong, and K. K. Tsia, "High-performance multi-megahertz optical coherence tomography based on amplified optical time-stretch," Biomed. Opt. Express **6**(4), 1340–1350 (2015).
7. W.-Y. Oh, B. J. Vakoc, M. Shishkov, G. J. Tearney, and B. E. Bouma, ">400 kHz repetition rate wavelength-swept laser and application to high-speed optical frequency domain imaging," Opt. Lett. **35**(17), 2919–2921 (2010).
8. V. Jayaraman, G. D. Cole, M. Robertson, A. Uddin, and A. Cable, "High-sweep-rate 1310 nm MEMS-VCSEL with 150 nm continuous tuning range," Electron. Lett. **48**(14), 867–869 (2012).
9. I. Grulkowski, J. J. Liu, B. Potsaid, V. Jayaraman, J. Jiang, J. G. Fujimoto, and A. E. Cable, "High-precision, high-accuracy ultralong-range swept-source optical coherence tomography using vertical cavity surface emitting laser light source," Opt. Lett. **38**(5), 673–675 (2013).
10. M. Y. Jeon, J. Zhang, Q. Wang, and Z. Chen, "High-speed and wide bandwidth Fourier domain mode-locked wavelength swept laser with multiple SOAs," Opt. Express **16**(4), 2547–2554 (2008).
11. H. Lim, J. F. de Boer, B. H. Park, E. C. Lee, R. Yelin, and S. H. Yun, "Optical frequency domain imaging with a rapidly swept laser in the 815-870 nm range," Opt. Express **14**(13), 5937–5944 (2006).
12. E. C. Lee, J. F. de Boer, M. Mujat, H. Lim, and S. H. Yun, "In vivo optical frequency domain imaging of human retina and choroid," Opt. Express **14**(10), 4403–4411 (2006).
13. U. Sharma, E. W. Chang, and S. H. Yun, "Long-wavelength optical coherence tomography at 1.7 microm for enhanced imaging depth," Opt. Express **16**(24), 19712–19723 (2008).

#279808 http://dx.doi.org/10.1364/BOE.8.001110
Journal © 2017 Received 1 Nov 2016; revised 20 Jan 2017; accepted 22 Jan 2017; published 25 Jan 2017

Biomedical Optics EXPRESS

14. S. K. Vashist, E. M. Schneider, and J. H. T. Luong, "Commercial smartphone-based devices and smart applications for personalized healthcare monitoring and management," Diagnostics (Basel) **4**(3), 104–128 (2014).
15. G. P. Agrawal, *Semiconductor Lasers*, 2nd ed. (Van Nostrand Reinhold, 1993), Chap. 7.
16. L. Fan, M. C. Wu, H. C. Lee, and P. Grodzinski, "10.1 nm range continuous wavelength-tunable vertical-cavity surface-emitting lasers," Electron. Lett. **30**(17), 1409–1410 (1994).
17. S.-S. Yang, J.-K. Son, Y.-K. Hong, Y.-H. Song, H.-J. Jang, S.-J. Bae, Y.-H. Lee, G.-M. Yang, H.-S. Ko, and G.-Y. Sung, "Wavelength tuning of vertical-cavity surface-emitting lasers by an internal device heater," IEEE Photonics Technol. Lett. **20**(20), 1679–1681 (2008).
18. S. Sakano, T. Tsuchiya, M. Suzuki, S. Kitajima, and N. Chinone, "Tunable DFB laser with a striped thin-film heater," IEEE Photonics Technol. Lett. **4**(4), 321–323 (1992).
19. E. Kapon and A. Sirbu, "Long-wavelength VCSELs: Power-efficient answer," Nat. Photonics **3**(1), 27–29 (2009).
20. Y. Liu, W. C. Ng, K. D. Choquette, and K. Hess, "Numerical investigation of self-heating effects of oxide-confined vertical-cavity surface-emitting lasers," IEEE J. Quantum Electron. **41**(1), 15–25 (2005).
21. K. H. Rhew, S. C. Jeon, D. H. Lee, B.-S. Yoo, and I. Yun, "Reliability assessment of 1.55-μm vertical cavity surface emitting lasers with tunnel junction using high-temperature aging tests," Microelectron. Reliab. **49**(1), 42–50 (2009).
22. J. Armstrong, M. Leigh, I. Walton, A. Zvyagin, S. Alexandrov, S. Schwer, D. Sampson, D. Hillman, and P. Eastwood, "In vivo size and shape measurement of the human upper airway using endoscopic longrange optical coherence tomography," Opt. Express **11**(15), 1817–1826 (2003).
23. A. C. Loy, J. Jing, J. Zhang, Y. Wang, S. Elghobashi, Z. Chen, and B. J. F. Wong, "Anatomic optical coherence tomography of upper airways," in Optical Coherence Tomography, W. Drexler, J. G. Fujimoto, eds. (Springer, 2015).
24. R. Chityala, C. Vidal, and R. Jones, "Utilizing optical coherence tomography for CAD/CAM of indirect dental restorations," Proc. SPIE **8566**, 85660A (2013).

1. Introduction

Since the first practical demonstration of swept-source optical coherence tomography (SS-OCT) [1,2], the performance enhancement and the expansion of the application fields have been fueled by development of various swept laser sources. A number of schemes have been proposed and deployed for higher imaging speeds [3–8], wider imaging ranges [8,9], finer resolutions [10], new wavelength bands [11–13], *etc.*, on the main engines of SS-OCT. Those advances have made the SS-OCT techniques more attractive and colorful for various fields of application. However, the costs of the SS-OCT systems are still high and have limited their applicability in many of potential areas. Including the time-domain or the spectral-domain OCT counterparts, most of the conventional OCT technologies are hardly suited to mobile healthcare units [14] or low-cost medical instruments for lowly developed countries. So far, the OCT systems require costly specialized elements such as a rapidly sweeping laser, high-resolution spectrometer or a broadband light source. The instrumentation costs cannot be greatly reduced until the economy of massive scale is established for them.

It is well known that a cheap single-mode laser diode such as a distributed feedback (DFB) laser has inherent wavelength-tuning capabilities [15]. Involved with the carrier density of the semiconductor, the injected-current dependence of the output wavelength is observed, but mostly too small to be utilized for a swept source. On the other hand, the temperature dependence is more considerable, typically given on the order of 0.1 nm/K's [15]. Owing to the variation of the refractive index by temperature, the optical path-length of the laser cavity can be tuned by heating or cooling the device. Presuming a practical temperature tuning range to be 100 K, wavelength sweeping of ~10 nm is readily obtainable in an economic way [16–18]. The critical drawback of the heater-based tunable laser is its low speed of operation. Heating or cooling a laser diode needs a time span far longer than milliseconds in most cases. Particularly, the active region of a typical edge-emitting laser diode is quite long and well connected to the substrate of the device. The speed of the thermal conduction for the bulky structure cannot be so fast and never fulfill the demand in the SS-OCT imaging. Nevertheless, it suggests that the operation speed could be largely enhanced if the heated volume were very small and loosely connected to the main body of the laser for fast and efficient heating.

Biomedical Optics EXPRESS

The vertical-cavity surface-emitting laser (VCSEL) has such a property which may provide a simple way of making a fast swept source by temperature tuning. The VCSEL is a type of laser diodes with a very short laser cavity formed by distributed Bragg reflectors (DBRs). It has a very thin active region sandwiched by the two DBR mirrors. Undesirably in high-power operations, the DBRs have poor thermal conductivities preventing the heat of the active region from easily dissipating through them [19]. As a consequence, temperature of the active region is easily increased by the internal heat sources. This results in extraordinary output characteristics. VCSELs look like having high dependence of operation wavelength on the injected current. This must not be confused with a purely current-involved effect. In fact, as more current is injected, the internal temperature of the active region is getting higher through the *self-heating* effect [19,20]. This temperature change finally produces a shift of operation wavelength. The self-heating effect has been routinely observed in the field of VCSEL research as one of the unwanted properties that limit the maximum output power. But it might give a straightforward and simple way of making a swept source.

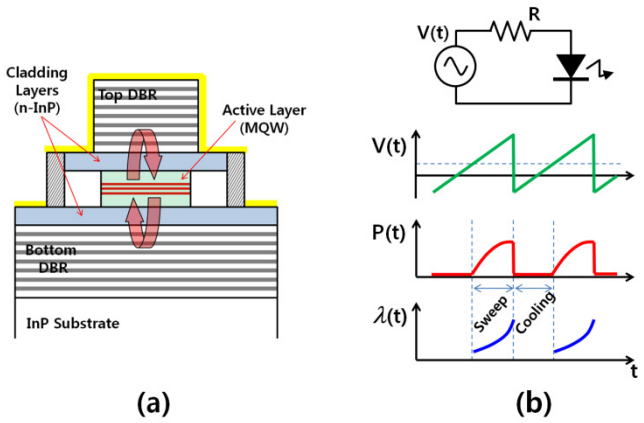

Fig. 1. Structure of the VCSEL device (a), and its response under pulse driving. Here, V(t), P(t) and λ(t) are the driving voltage, the optical output power and the output's wavelength in time, respectively.

In this study, we took advantage of the self-heating effect for sweeping the output wavelength. By electrically driving a VCSEL in a proper manner, a useful swept source for SS-OCT was realized in a surprisingly simple way. Our source should not be confused with a MEMS-based VCSEL device in which a micro-electromechanical mirror tunes the cavity length in a mechanical manner [8,9]. For our making a swept source, no internal or external mechanics was involved. In our study, we utilized a VCSEL diode laser that has a conventional device structure of undercut quantum wells [19]. Figure 1 shows the schematic device structure (a) and the output response of the VCSEL when driven by a sawtooth current (b). Inside the VCSEL device, the active layer of multiple quantum well (MQW) is placed between the semiconducting cladding layers. They give current injection pathways, simultaneously acting as major heat dissipating routes to the external metal contacts. The active MQW is electrically and thermally isolated in the transverse plane. The vertical heat conduction throughput is also low because of the cladding's thinness. After all, the active region is easily heated by the injected current. This gives a suitable type of VCSELs to make a self-heating-induced sweep. As the VCSEL diode is driven by sawtooth-like current pulses as illustrated in Fig. 1(b), the temperature gradually increases and the wavelength (λ) is continuously swept accordingly. A cooling period of low or no currents below the laser's threshold is necessary because no active cooling mechanism is utilized inside the device. Our

Biomedical Optics EXPRESS

self-heating sweep VCSEL (SS-VCSEL) is a VCSEL source driven in an optimal way of producing a wavelength-swept output in this principle of operation.

In this report, development of the SS-VCSEL source is fully described focused on introducing a new low-cost swept source for SS-OCT imaging. Various characteristics of the VCSEL in a sweep operation mode were investigated for the purpose. Basic imaging performances of the SS-OCT system were evaluated to find the feasibility. It was found that our SS-VCSEL may give OCT imaging performances acceptable or promising for some of specialized OCT applications. The maximum effective sweep rate was found to be between 10 kHz and 100 kHz. The full bandwidth of sweep was 10 nm, supporting an axial resolution of 135 μm in air. The maximum imaging range was longer than 10 cm, which is a very attractive feature for long-range OCT imaging. Notice that, in our study of SS-VCSEL, we utilized a VCSEL commercially available in the market. The unit price is no more than a hundred US dollars and can be even lower in large quantities. No additional optical or mechanical element was added except for the driving electronics. According to the best of our knowledge, this gives the least expensive solution for SS-OCT instrumentation.

2. Properties of the VCSEL

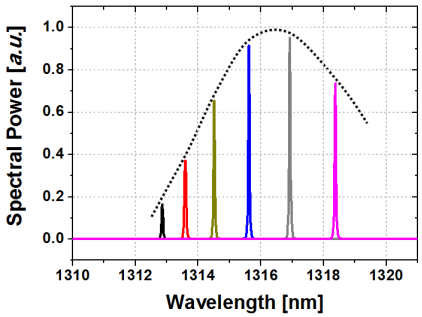

Fig. 2. Spectra of the VCSEL's output in CW operation with various currents: I_V = 2, 4, 6, 8, 10 and 12 mA from the left.

The basic properties of the VCSEL device were evaluated before making our swept source. The VCSEL device used in this study was originally developed for a telecom laser source operating in the 1.3-μm wavelength band (RC22xxx1-F, Raycan, South Korea). According to the manufacturer's information, the basic device structure was the same as given in Fig. 1(a) [21]. In our experiment, the optical spectra of the VCSEL's output were measured with an optical spectrum analyzer (OSA) in DC and AC electric driving conditions. For current regulation, an electric resistor of R = 200 Ω was placed in series with the VCSEL laser diode. The injected current, I_V, could be monitored by the voltage across the resistor. At first, the temperature-wavelength coefficient was evaluated. Changing the case temperature of the VCSEL in a range of 3 to 24°C, the peak wavelength of the laser was measured while keeping the injected current constant. The coefficient was measured to be 0.08 nm/K. This matches a typical value of the single-mode laser diode operating at the wavelength band. In the next, the self-heating effect and the consequent wavelength variation by injected current were tested. Figure 2 shows the optical spectra of the continuous-wave (CW) operation mode in DC current driving. It depicts the spectra of I_V = 2, 4, 6, 8, 10 and 12 mA for the peaks from the left. The measurement result clearly showed an apparent dependence of the wavelength on the injected current. The output power of the VCSEL reached its peak at I_V = 10 mA and decreased monotonically at higher currents. It was explained by the self-heating effect. The quantum yield of radiative transitions drops by the rise of phonon-involved processes in the active region after being self-heated by the current.

Biomedical Optics EXPRESS

The dynamics of the self-heating effect was investigated in AC current driving condition. Rectangular current pulses of 50% duty ratio were injected into the VCSEL while keeping a constant pulse amplitude, 4 mA. Both the low and the high sides of the pulse's current were above the threshold current. The output spectrum of the VCSEL was measured with the OSA at each pulse frequency. The measurement was repeated as varying the frequency, *f*, from 10 Hz through 1 MHz. Figure 3 shows the resulted spectra of different driving frequencies (a), and the wavelength separations, Δλ, measured as a function of frequency (b). As seen in Fig. 3(a), each output spectrum produced two peaks at the spectral edges when operated at a low frequency (<100 kHz). In the pulsed operation, the temperature of the active region must have followed the current variation, alternating between two distinct points. However, the peaks became less clear at higher frequencies, probably due to the transient responses of the internal temperature variations. Here, the peak wavelength separation, Δλ, was found in each spectrum. It could be regarded as a transfer function of the VCSEL's current-to-wavelength conversion in the self-heating sweep (SS) operation. The small-signal response could tell the operation speed limit in a linear-system approximation. The measurement result of Fig. 3(b) suggests that the speed of wavelength tuning by current modulation was limited by a relatively slow dynamics that occurred in a few tens of microseconds. Certainly, this could not be the fast carrier dynamics involved with the current by itself. It was better explained to be driven by the thermal effect. And the thermal dynamics was thought to be exceptionally fast in the VCSEL due to the unique device structure. From the result shown in Fig. 3(b), the maximum sweep rate would be expected to be around 100 kHz estimated in a linear-system approximation, if a decrease in sweep bandwidth by 50% could be accepted. It would be 40 kHz if an optical bandwidth loss of 30% was allowed.

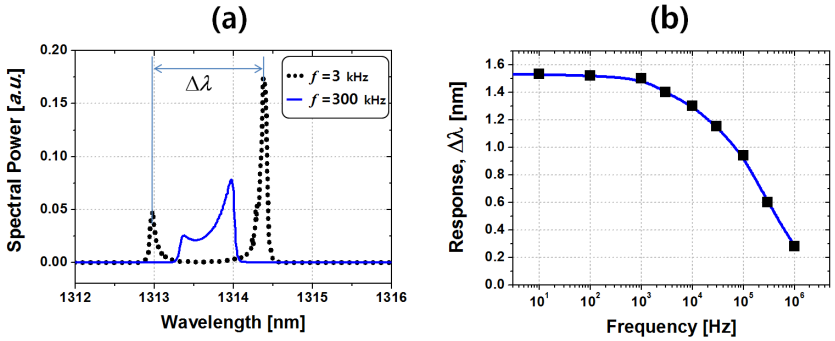

Fig. 3. Spectra of the VCSEL's output when driven by rectangular current pulses of different driving frequencies (a), and the wavelength separation of the spectral peaks, Δλ, which was obtained in each spectrum as a function of driving frequency, *f* (b). In Fig. 3(b), the blue line is the curve fit of the measured values denoted by square dots.

3. SS-VCSEL swept source

Our SS-VCSEL source was constructed based on the information found by the VCSEL's basic properties. We chose a sawtooth waveform for the current pulse applied to the device with a proper DC bias. To allow a sufficient cooling period, a duty ratio of 50% was given to the laser's output power. This could be obtained by adjusting the DC current. The driving frequency was set to f = 5 kHz for the best bandwidth, and f = 40 kHz for the best speed operation. Those two driving conditions would be compared in performance. Here, it is worth noting that the true effective sweep rates of our SS-VCSEL were twice the nominal speeds because of the 50% duty ratio. By employing two SS-VCSELs that operate in parallel, doubled sweep rates could be obtained in an alternating operation. The case temperature of our VCSEL was actively cooled down and kept constant at 3°C (± 1°C) for a wider bandwidth. The effect of the case cooling will be discussed later in this report. The average

Biomedical Optics EXPRESS

optical power of the laser was 412 μW and 472 μW for f = 5 kHz and f = 40 kHz, respectively. To measure the sweep characteristics, an interferometric measurement was needed for the spectral fringe analysis. We built an SS-OCT system for this purpose and it was used as the imaging system later as well. Figure 4 shows the schematic of the SS-OCT system constructed with our SS-VCSEL source and a fiber-optic 3-dB coupler. This simple Michelson-type configuration of SS-OCT gave minimal complexity but naturally exhibited a decreased power efficiency with a sensitivity penalty. But it was acceptable for the purpose of evaluating the basic performance of our SS-VCSEL.

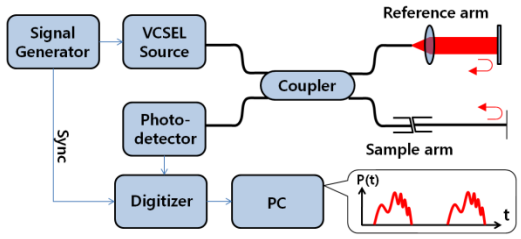

Fig. 4. Schematic diagram of the simple SS-OCT system with our SS-VCSEL source.

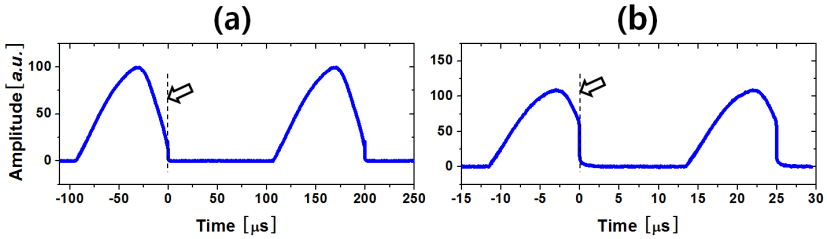

Fig. 5. Optical power of the SS-VCSEL's output when driven at f = 5 kHz (a), and f = 40 kHz, respectively.

Figure 5 shows the detected power waveform of the VCSEL's optical output in the SS operation modes of f = 5 kHz (a) and f = 40 kHz (b), respectively. Those outputs were obtained by sawtooth pulses with upward current ramps (↗). As indicated by an arrow in each plot of Fig. 5, the origin of the time coordinate (t) was set to be at the falling edge for each outputted laser pulse, *i.e.*, at the end of each current ramp. In an operation cycle, there were a laser sweep period (t<0) and a cooling period of no output power (t>0) that make up a pulse's duty ratio of 50%. The optical spectra of the SS-VCSEL's outputs are shown in Fig. 6 for the two driving conditions. The full optical bandwidth was 10 nm for f = 5 kHz while it was 7 nm for f = 40 kHz. For those two conditions, the same amplitudes and bias currents were applied while switching the frequency. Because of the limited speed of heating and cooling in the self-heating process, the SS-operation bandwidth decreased in the high-frequency regime. This result well agreed with the property of the VCSEL observed in Fig. 3(b).

The interferometric SS-OCT system was used to find the sweep characteristic of our SS-VCSEL. In a sweep period, the wavelength was continuously changed with a non-zero optical power. This sweep could be expressed with wavenumber, $k = 2\pi/\lambda$. The time-to-k map, so called t-k conversion map, defines the relation of the two domains for the VCSEL's pulsed sweep. In our experiment, the map was obtained by acquiring the spectral interferogram with the SS-OCT system. For this, an isolated single reflection point was located on the sample arm at a known position. By help of Hilbert transform, the t-k conversion map was extracted so that the resampled k-domain interferogram appeared as a sinusoid of a given frequency. Figure 7 and Fig. 8 show the acquired raw interferograms (a), the measured t-k conversion

Biomedical Optics EXPRESS

maps (b), and the resampled interferograms in the *k* domain (c) for the two operation conditions of *f* = 5 kHz and *f* = 40 kHz, respectively. In this measurement, the reflection point on the sample arm was placed 5.0 mm apart from the origin, *i.e.*, the conjugated position of the reference mirror. As seen in Fig. 7(b) and Fig. 8(b), the sweep operation observed in the *t*-*k* map was continuous over the full bandwidth. But it was obviously not a linear sweep. The *k*-tuning speed was getting faster to the end of each sweep. It could be explained by the fact that the heating rate must have been accelerated as the temperature increased.

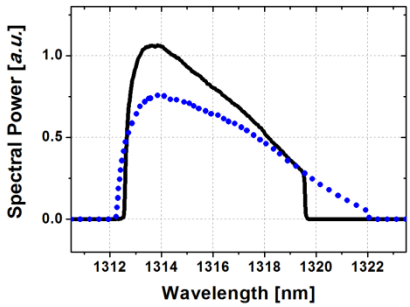

Fig. 6. Output spectra of the SS-VCSEL driven at *f* = 5 kHz (dots) and *f* = 40 kHz (line), respectively.

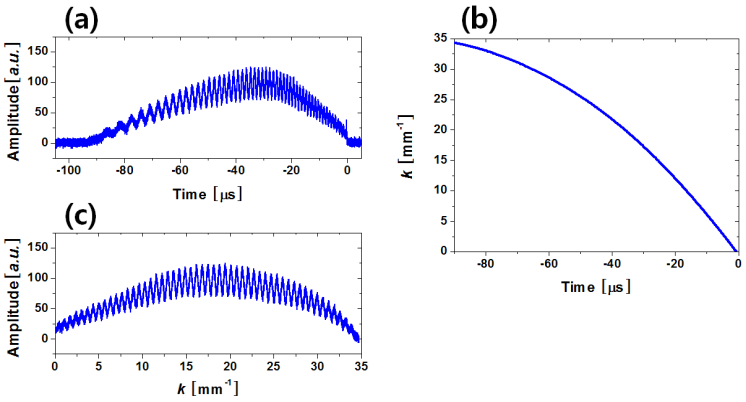

Fig. 7. Raw time-domain interferogram (a), the *t*-*k* conversion map (b), and the resampled *k*-domain interferogram (c), respectively, obtained with our SS-VCSEL driven at *f* = 5 kHz.

Biomedical Optics EXPRESS

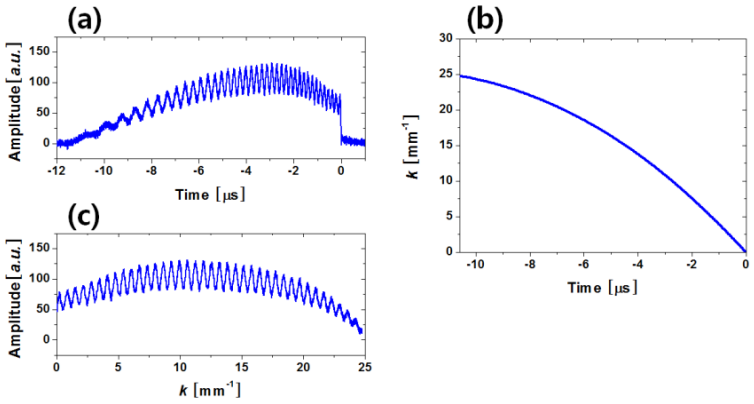

Fig. 8. Raw time-domain interferogram (a), the *t*-*k* conversion map (b), and the resampled *k*-domain interferogram (c), respectively, obtained with our SS-VCSEL driven at f = 40 kHz.

4. Imaging performance

The OCT imaging performance was evaluated for the SS-OCT system utilizing our SS-VCSEL swept source. The axial point spread functions (PSFs) were obtained as changing the position of the reference reflector. The axial resolutions and the sensitivities were estimated from the PSFs. Figure 9 shows the measurement results for the case of f = 5 kHz (a), and f = 40 kHz (b), respectively. Here, z on the horizontal is the positional axis of the inverse-*k* domain. The sample reflector used for this measurement made a constant reflection of –35.4 dB. The reflected power and the state of the polarization were readjusted every time after changing the position. An optical power-meter and a polarization controller were used for this. Here, the axial resolution was defined by the full width of the PSF at the power level of –6 dB in respect to the peak power. For our OCT system, the axial resolution was found to be 135 μm and 170 μm in the cases of f = 5 kHz and f = 40 kHz, respectively. This corresponds to resolutions of 96 μm and 121 μm in typical tissues samples (n = 1.4). The obtained resolutions nearly matched the transform-limited performance. The overall resolving power was somehow disappointing, roughly ten times lower than those of the current OCT technologies. It was naturally due to the narrow bandwidth of our source.

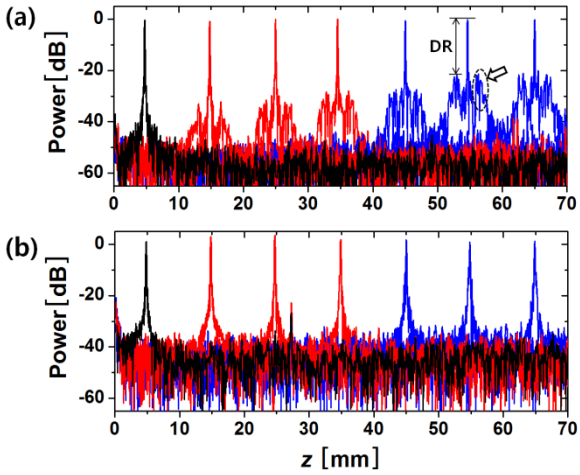

Fig. 9. Axial PSFs of the system for the cases of f = 5 kHz (a) and f = 40 kHz (b), respectively.

Biomedical Optics EXPRESS

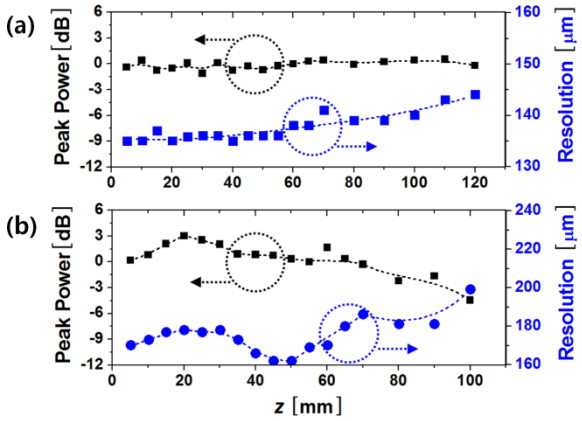

Fig. 10. Peak power and the resolution of the PSF as functions of the axial position for the cases of f = 5 kHz (a) and f = 40 kHz (b), respectively.

The system sensitivity was evaluated to be −91.0 dB for the case of f = 5 kHz, and −82.6 dB for f = 40 kHz, respectively, with the sample-arm powers of 192 μW and 223 μW. Note that the sensitivity is proportional to the optical power. For our system, it could be better than −100 dB if the sample-illuminating power were more than 2 mW in the case of f = 5 kHz. Still, practical OCT imaging was obtainable without a power booster amplifier for our swept source. The variation of resolutions and peak powers of the PSF along the axial position of the reflector, denoted by z, were summarized in Fig. 10. The imaging range was found to be very wide due to the superior instantaneous linewidth of our laser source. In the case of f = 5 kHz, the peak power roll-off was no more than 2 dB up to 100 mm allowing an exceptionally wide imaging range of OCT. In the case of f = 40 kHz, significant peak power drops and the resolution degradation were observed in z>70 mm. It could be explained by the limited bandwidth of our photodetector used in the system. For both the cases, the maximum imaging range was longer than 100 mm, defined by the 6-dB sensitivity roll-off limit.

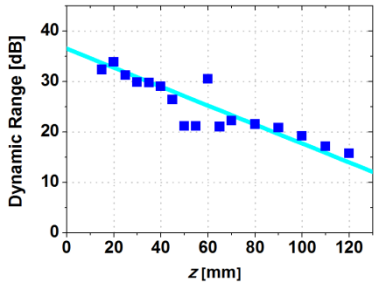

Fig. 11. Measured dynamic range of the system as a function of the axial position for the case of f = 5 kHz.

Biomedical Optics EXPRESS

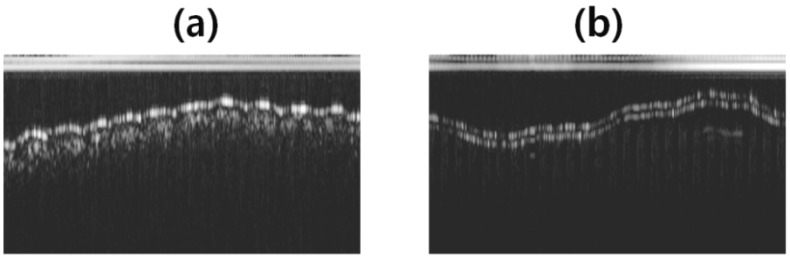

Fig. 12. OCT images of a human fingertip (a) and a 150-μm thick glass plate (b), respectively, acquired in 0.4 second. The full depth of the vertical dimension was 5 mm in air.

In the case of f = 5 kHz, the imaging range was, however, restricted by the dynamic range. As indicated by an arrow in Fig. 9(a), the main lobe of the PSF was followed by spurious responses in the both sides. This type of sidelobes were not observed for z<10 mm. However, for the PSFs of z>10 mm, they grew stronger as the position got farther. Those noise-like signals might overwhelm the weak real signals in the vicinity of a strong peak. And this effect definitely limited the dynamic range of the system. The dynamic range (DR) was measured by the ratio of the peaks between the main lobe and the sidelobes of a PSF as illustrated in Fig. 9(a). Figure 11 shows the dynamic range variation along the axial position for f = 5 kHz. Assuming the minimum acceptable dynamic range is 20 dB in practical OCT imaging, the imaging range reduced to 90 mm. This problem of the dynamic range reduction was not observed in the case of f = 40 kHz. The cause of those spurious sidelobes and the reason why they appeared only in the low-speed operation were not found in this study and remained for the future investigation.

Finally, OCT imaging test was performed with our SS-OCT system. A one-axis beam scanner was equipped at the sample arm. OCT images were acquired while the SS-VCSEL was operated at f = 5 kHz. Figure 12 shows OCT images of a human fingertip (a), and a 150-μm thick glass plate, respectively, obtained with our SS-OCT system. Compared to popular OCT images of human fingertips available in the literature, the image of Fig. 12(a) is largely blurred in the vertical direction because of the low axial resolutions. The dermis and epidermis layers were still resolved. In Fig. 12(b), the front and back planes spaced by 150 μm in glass were well resolved as well. Concerned with the axial resolutions, our SS-OCT seems unsuitable for typical applications of high-resolution imaging at the current stage.

5. Discussion

The overall performance characteristic of our SS-VCSEL has been found quite different from the conventional types of swept sources. It can be summarized to a relatively poor resolution, a long image range and a low power. The power can be easily boosted by a semiconductor optical amplifier (SOA) in moderate costs. Due to the wide imaging range, our SS-VCSEL can be suitable for applications such as the anatomical OCT that visualizes the internal anatomy of hollow organs in a relatively large scale [22,23]. It can be suited for some of dental applications such as an intraoral 3D scanner [24] as well as the industrial 3D scanners. Taking advantage of the inexpensiveness, our SS-VCSEL may help explore non-conventional applications that the current OCT technologies have practically neglected due to the cost-related issues.

The axial resolution of our SS-VCSEL is too poor to be useful in most of medical applications. It may need enhancements by a factor of 3 or 4 at least. There are two possible ways of extending the bandwidth in our SS-VCSEL: deep cooling and bandwidth combination. In the temperature range of our SS-VCSEL operation, the upper limit was involved with the quantum yield drop due to the non-radiative recombination of carriers. And the lower limit was the case temperature. Cooling the device's case gives a gain of bandwidth

Biomedical Optics EXPRESS

by 0.08 nm/K. We experimentally confirmed that cooling the laser case down by 21 K beneficially increased the sweep bandwidth by + 1.8 nm through allowing a higher current at the peak. In a simple math, a bandwidth enhancement factor of 2 might be realized by deeply cooling the VCSEL by 125 K but, obviously, with costs of massive cooling mechanism. In our experiments, we kept our VCSEL's case at 3°C, ~20 K lower than the room temperature. This gave us a gain of + 1.6 nm. Cooling by −20 to −30 K can be practical due to inexpensive thermoelectric coolers (TECs). Further enhancement by deep cooling seems unpractical in terms of cost-effectiveness at the current stage. On the other hand, multiple VCSELs of slightly different operation wavelengths could cooperate for a wider combined bandwidth. For example, four VCSELs with a wavelength spacing of 8 nm could be arrayed in parallel to generate their own sweeping pulses. The outputs from the different lasers could be optically combined in temporally interleaving the pulses. It could give time-domain multiplexing of multiple bands. Then, the full bandwidth of the combined sweep could be as wide as ~32 nm. This could possibly meet the demand of most low-cost medical imaging systems.

The performance improvement could be achieved by optimization of the device structure or the materials used in VCSEL. The thermal conduction capability is involved with heating and cooling rates. If too high, the active region will be heated too slow, but cooled so fast. If too low, vice versa. There must be an optimum level of thermal conductivity for best speeds operation. Applying temperature-sensitive materials in VCSEL could increase the bandwidth of sweep. The material selection for the active region has low degree of freedom. But, for the surrounding cladding layers or the DBR layers, better materials might be selected that exhibit a higher temperature-index coefficient for a wideband operation.

A critical factor on the practical applicability of our technique in the real-world systems is the long-term reliability of our light source. To get the maximum sweep bandwidth in our experiments, the injected currents to the VCSEL slightly exceeded the absolute maximum rating of the manufacturer's data, particularly at the peaks of the current ramps. The peak current (19 mA) was roughly two times higher than the recommended value of injection current while the average was still in the reliable operation range. In a rough estimation, the core of the VCSEL device repeatedly experienced temperature variations of 125 K (10 nm / 0.08 nm/K) at high cycling frequencies. The average temperature did not exceed the recommended operation range. But the frequent changes of the temperature might apply dynamic stress to the semiconductor structure and could potentially degrade the performance after a long time of operation. We tested the reliability of our SS-VCSEL by a continuous long-term operation. Figure 13 shows the measured output power variation of our SS-VCSEL. During the test of 230 hours, no considerable decrease in output power was observed as well as in axial resolution of the OCT system. A slight deviation of power could be explained by the case temperature variation of ± 1.5 K around 3°C observed in our test. It is, yet, insufficient to make a final conclusion on the long-term reliability and needs further systematic investigation. But the test result gave a positive sign on the reliable operation of our SS-VCSEL.

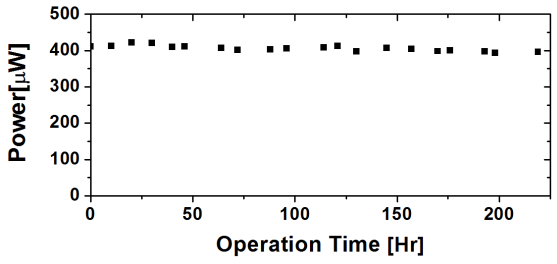

Fig. 13. Output power variation of the SS-VCSEL running at f = 5 kHz. Notice that no significant decay was observed within 230 hours of continuous operation.

Biomedical Optics EXPRESS

6. Conclusion

In this report, we introduced a new swept source for SS-OCT that can be useful in cost-sensitive applications. In our SS-VCSEL, a VCSEL diode laser was directly modulated by current pulses. The self-heating effect brought a wavelength shift in accordance to the temperature rise caused by the injected current. The self-heating sweep produced a continuous modulation of the laser light in optical frequency. We tested various properties of our SS-VCSEL light source. Our source was found to provide interesting characteristics. The maximum sweep bandwidth was 10 nm that supported an axial resolution of 135 μm in SS-OCT. The instantaneous linewidth was so fine that an imaging range of ~10 cm could be supported. The OCT imaging test verified that our source could be used in SS-OCT imaging despite the narrow bandwidth. The inherent weakness of narrow bandwidth and low power is expected to be alleviated by further studies and improvements. Obviously, our SS-VCSEL can hardly become a versatile source for all the OCT applications. But it seems attractive and considerable in some specialized areas where instrumentation costs or imaging ranges are the main issues.

Funding

This research was supported by the Basic Science Research Program through the National Research Foundation of Korea (NRF-2014R1A1A1006183).